The Compact Muon Solenoid Experiment

CMS Draft Note

Mailing address: CMS CERN, CH-1211 GENEVA 23, Switzerland

2011/03/24
Head Id: 37835
Archive Id: 29932:47167P
Archive Date: 2011/02/08
Archive Tag: trunk

Search For Resonant Production of Lepton Jets

J. Pivaski, A. Safonov, A. Tatarinov and The CMS Collaboration
Texas A&M University

Abstract

A signature-based search for groups of collimated muons (muon jets) is performed using 35 pb^{-1} of data collected by the CMS experiment at the LHC, at a center-of-mass energy of 7 TeV. The analysis aims to search for production of new low-mass states decaying into pairs of muons, and is designed to achieve high sensitivity to a broad range of models predicting muon jet signatures. With no excess observed in the data over the background expectation, upper limits on the production cross section times branching ratio times acceptance are derived for several event topologies and range from 0.1-0.5 pb. in addition, the results are interpreted for several benchmark models in the context of SUSY with a new light dark sector yielding limits on new physics production exceeding the Tevatron reach.

1 Introduction

Recent astrophysical observations implying excess of high energy positrons in the cosmic ray spectrum [1] have motivated the rise of new physics scenarios suggesting that this excess may be associated with the annihilations of the dark matter particles [2]. In these models the annihilation of a TeV-scale dark matter in the galactic halo accounts for the anomalous excess of cosmic ray leptons and accommodates discrepancies in direct searches for dark matter [3]. One realization of such models assumes an extra $U(1)$ gauge symmetry with weak coupling to the Standard Model (SM). The $U(1)$ symmetry is broken, leading to a light massive vector boson ($m \sim O(1\ \mathrm{GeV}/c^2)$), a "hidden" or "dark" photon, which can have a small kinetic mixing with the SM photon providing a portal for the hidden sector photon to decay to leptons and, if kinematically allowed, hadrons. More complex models can lead to a whole hierarchy of the dark sector states. Hidden sectors can be naturally realized in supersymmetric models where coupling of the dark sector to the SUSY sector can be enhanced. At the LHC, if the energy is sufficient for producing SUSY particles, these models predict production of "dark photons" as part of the SUSY cascades. Such dark photons would decay to pairs of leptons and/or hadrons via kinetic mixing with photons or, in more complex scenarios, can have preferential coupling to leptons [4]. Assuming moderate coupling strength of the hidden sector to the SUSY sector, the new light hidden states may be produced in decays of the lightest SUSY particle (LSP), e.g. the lightest neutralino as in the case of the Minimal Supersymmetric Model (MSSM) extended by the hidden dark sector. The lightest neutralino can decay either entirely to the light hidden sector particles and sparticles while a heavier dark fermion providing the cold dark matter candidate, or to light hidden particles and a dark neutralino [5], which becomes the new cold dark matter candidate. Because the LSP in these models is no longer stable, there are scenarios [6] where the squark is chosen to be the LSP, which would decay into the light hidden sector states. Depending on the complexity of the dark sector, at the LHC one may expect cascade decays of the light hidden states with emission of multiple dark photons leading to characteristic "lepton jet" signatures.

A similar signature involving production of new light bosons decaying to pairs of leptons is predicted in the context the Next-to-MSSM (NMSSM) models [7–13], which extend MSSM by new singlet superfield weakly coupling to the standard MSSM sector. Compared to the MSSM, the NMSSM greatly reduces the fine-tuning and provides an elegant solution for the "μ-problem" [14]. The NMSSM has an expanded higgs sector and provides new decay modes for the SM-like higgs h_1 to a pair of the new light CP-odd higgs states, a_1, significantly weakening higgs mass limits from direct searches at LEP [15]. If $m(a_1) < 2m(\tau)$, there is a substantial branching ratio for $a_1 \to \mu\mu$ decays leading to similar "muon jet" signatures.

While previous searches [16, 17] for lepton jets in the context of SUSY with a dark sector at the Tevatron did not observe signals of the new physics consistent with the topology of lepton jets, the lower center of mass energy may make these signatures inaccessible. Similarly, the sensitivity of the Tevatron search [18] for $h_1 \to a_1 a_1 \to 4\mu$ is very limited and has a small impact on the allowed NMSSM parameter space [19]. Due to the high center-of-mass energy, the LHC may provide access to production of these new states with even relatively small amounts of data motivating searches for anomalous production of collimated groups of leptons in the early LHC data. This note describes a signature-based search for production of new light resonances decaying to pairs of muons using the first 35 pb^{-1} of data collected by the CMS experiment during the 2010 LHC run. The results allow a model-independent interpretation as well as set limits on specific benchmark scenarios in the context of SUSY and NMSSM Higgs described in [5, 6] and [19], respectively.

2 The Dataset and Trigger

The CMS is a general purpose detector providing excellent momentum and direction measurements of particles produced in pp collisions of the LHC beams. The central feature of the Compact Muon Solenoid (CMS) apparatus is a superconducting solenoid of 6 m internal diameter. Within the field volume are the silicon pixel and strip tracker, the crystal electromagnetic calorimeter (ECAL) and the brass/scintillator hadron calorimeter (HCAL). Muons are measured in gas-ionization detectors embedded in the steel return yoke. In addition to the barrel and endcap detectors, CMS has extensive forward calorimetry. CMS uses a right-handed coordinate system, with the origin at the nominal interaction point, the x-axis pointing to the center of the LHC, the y-axis pointing up (perpendicular to the LHC plane), and the z-axis along the anticlockwise-beam direction. The polar angle, θ, is measured from the positive z-axis and the azimuthal angle, ϕ, is measured in the x-y plane. The pseudorapidity $\eta = -\ln(\tan\theta/2)$ is frequently used instead of the polar angle θ. Here we only briefly describe the components of the CMS directly relevant to this analysis, the full details of the detector, its subsystems and performance is described elsewhere [20].

The inner tracker measures charged particles within the pseudorapidity range $|\eta| < 2.5$. It consists of 1440 silicon pixel and 15 148 silicon strip detector modules and is located in the 3.8 T field of the superconducting solenoid. It provides an impact parameter resolution of ~ 15 μm and a transverse momentum (p_{T}) resolution of about 1.5 % for 100 GeV/c particles. The muons are measured in the pseudorapidity window $|\eta| < 2.4$, with detection planes made of three technologies: Drift Tubes, Cathode Strip Chambers, and Resistive Plate Chambers. Matching the muons to the tracks measured in the silicon tracker results in a transverse momentum resolution between 1 and 5 %, for p_{T} values up to 1 TeV/c.

Because of the high rate of the collisions, the CMS uses a two-level dedicated trigger system. The first level (L1) of the CMS trigger, composed of custom hardware processors, is designed to select, in less than 1 μs, the most interesting events, using information from the calorimeters and muon detectors. The High Level Trigger (HLT) processor farm, running a simplified and highly optimized version of the CMS offline reconstruction, further decreases the event rate from up to 100 kHz to 100 Hz, before data storage.

The data used in this analysis have been collected by the CMS experiment during the 2010 run of the LHC at the center-of-mass energy of 7 TeV and corresponds to the luminosity of 35 ± 1.4 pb^{-1}. The data have been collected using inclusive non-isolated muon triggers with the lowest available p_T threshold. In Level 1, the data are selected using muon candidates reconstructed by the L1 muon hardware followed by the confirmation at the HLT, where muons are reconstructed by matching standalone muon tracks with the tracks reconstructed in the silicon tracker detectors to refine the muon transverse momentum p_T measurement. Because the trigger configuration was changing during the data taking period, there are three distinct parts of the dataset where the triggers used had transverse momentum thresholds of 9, 11 and 15 GeV/c at the HLT. In all cases, Level 1 thresholds were low enough to ensure that the HLT thresholds are at the plateau of the Level-1 muon efficiency. To make the selected data uniform, we additionally require offline events to contain at least one trigger candidate with $p_T > 15$ GeV/c as measured online, such that the final dataset is the same as it would be as though it had been collected using a single inclusive muon trigger with $p_T > 15$ GeV/c.

3 Offline Selections and Analysis of the Data

In this analysis we search for evidence of new light bosons decaying into pairs of muons. The new particles can be isolated or produced in groups, coming from cascade decays in the new sector ending with several instances of the lowest-state particle. In addition to di-muon decays, the new particle decay channels can include pairs of electrons and perhaps hadrons. In many scenarios, multiple instances of such new boson can be produced per event. This analysis is therefore searching for one of more pair of muons with the invariant mass consistent with being produced in the decays of the same particle. Assuming on-shell production of at least a fraction of these new bosons per event, the new physics would manifest itself as enhancement in the rate of production of muon pairs consistent with a certain common mass.

We attempt to achieve a balance of two important goals. First, to achieve high sensitivity for a representative range of specific new physics scenarios leading to characteristic muon jet signatures and, second, to present results that would allow future interpretation in the context of other models of new physics yielding lepton jet signatures. Essentially all classes of models of new physics relevant to this analysis lead to the production of events of several different topologies in terms of the number of collimated muon jets and multiplicities of muons within each jet. Because these topologies have different sources and levels of SM backgrounds, we categorize events using topologies with different expected signal-to-background ratios to maximize the overall sensitivity of the analysis. Achieving the second goal requires minimal dependence of acceptance on the details of a specific model, which often arise due to detector inefficiencies that can be difficult to parameterize in a fully generic way.

In the offline analysis, events are required to have at least one primary vertex reconstructed in the luminous region along the beamline to minimize background events not originating from collisions. Selected events are further required to have at least one high quality muon candidate with $p_T > 15$ GeV/c matching the muon selected in the online trigger and within $|\eta| < 0.9$ reconstructed using an inside-out algorithm, which ensures high efficiency in the environment with multiple nearby muons. This algorithm extrapolates tracker tracks into the muon system and attaches individual tracklets (stubs) reconstructed in muon chambers. The assignment is arbitrated in the sense that any stub in the muon system can only be associated with one extrapolated tracker track most compatible with the stub. The reconstructed muon candidate is required to have stubs in at least two out of four muon stations it crosses. To be classified as high-quality, muon candidates are required to have at least eight hits in the silicon tracker. The requirement of $|\eta| < 0.9$ is necessary to ensure high and well understood trigger efficiency insensitive to the presence of muon hits from other nearby muons expected in the signatures with collimated muons. It avoids the endcap region where trigger efficiency can be substantially diminished in the presence of multiple closely spaced muons due to the features of the trigger electronics setup. Additional muon candidates are required to have $p_T > 5$ GeV/c, to be contained within $|\eta| < 2.4$, and to satisfy the same quality requirements.

Muon jets are reconstructed by iteratively clustering muon candidates starting with one of the muon candidates. Each additional muon is added to the jet if the invariant mass of the new muon and any opposite charge muon already assigned to the jet satisfies $m(\mu,\mu) < 9$ GeV/c^2 and is compatible with originating from the same vertex (confidence level of the vertex fit $>$ 1%). This clustering procedure always converges and is independent of the order in which muons are added to muon jets. The choice of $m(\mu,\mu) < 9$ GeV/c^2 ensures that muons originating from the same b-quark are always clustered into the same muon jet and most muons originating from different b-quarks are clustered into different muon jets. It is also appropriate for topologies predicted by most relevant models of new physics, as the typical masses of the

heavier hidden states originating the cascades are of the order of a few GeV/c^2. Note that the efficiency of the clustering algorithm does not depend on the boost of the muon jets, thereby reducing the sensitivity of the analysis to the details of the kinematics that can differ from one model to another. As a consequence of the clustering algorithm, each muon jet must contain at least one muon of each charge, but can contain arbitrarily many muons. Within each muon jet, we identify the pairs of muons that are most likely to have arisen from individual dark photon decays by assigning pairs of oppositely charged muons with minimal difference in dimuon mass (since all instances of the dark photon have the same mass). We refer to such pairs as fundamental dimuons.

All events are then categorized according to the number of muon jets N and the number of muon candidates n_i in the i^{th} muon jet, thus forming topologies denoted as $R^N_{n_1 \ldots n_N}$. In topologies with multiple dimuon candidates, the reconstructed masses of all fundamental dimuons would be consistent with each other within detector resolution for signal events, but not necessarily for backgrounds. Therefore, we build a K-dimensional distribution of reconstructed dimuon masses $m_1, ..., m_K$ for each topology, where K is the number of reconstructed dimuons per event. The signal of new physics would appear as a striking enhancement of events at a point near the K-dimensional diagonal with $m_1 \sim ... \sim m_K \sim m_0$, where m_0 is the mass of the new particle. While the distributions of background events are not smooth due to low-mass resonances, the background distributions extend beyond the diagonal in a known way. If such enhancement were to be observed, one can further construct the invariant mass of combinations of dimuons in the same muon jet to search for possible structure, e.g. a process of the type $a_2 \to a_1 a_1 \to (\mu\mu)(\mu\mu)$ would lead to an enhancement in the invariant mass of pairs of dimuons consistent with $m(a_2)$. The only exception is the R^1_2 topology with exactly one fundamental dimuon per event: the signal would appear as a narrow peak in the 1D distribution of dimuon mass m. For topologies with K dimuon candidates, we define the signal region as a "corridor" near the diagonal in the K-dimensional space of width $5 \times \sigma(m)$, where $\sigma(m) = (0.026 + 0.0065\, m)$ GeV/c^2 (for barrel $|\eta^{\mu\mu}| < 0.9$) and $(0.026 + 0.013\, m)$ GeV/c^2 (for endcap $0.9 < |\eta^{\mu\mu}| < 2.4$). The parameterization for $\sigma(m)$ was derived from studies of J/ψ, ψ', ϕ, ρ/ω, and η (decays to $\mu\mu\gamma$) resonances and high-p_T Monte Carlo simulations, and corresponds to the resolution expected of hypothetical dimuons with $p_T \sim 300$ GeV/c in the barrel region and $p_T \sim 150$ GeV/c in the endcap. After the shape of the background events distribution in the K-dimensional space is measured, the data in the off-diagonal part can be used to obtain the background normalization, which can then be used to fit the data in the near-diagonal region for signal plus background.

Event topologies $R^N_{n_1 \ldots n_N}$ have different rates and compositions of the SM backgrounds. The single-dimuon topology R^1_2 suffers from a particularly high rate of the SM backgrounds due to $b\bar{b}$ and Drell-Yan processes. Without additional selections, the SM backgrounds would be too large to maintain sensitivity to signals with picobarn-scale cross-sections. To reduce the SM backgrounds, events in the R^1_2 topology are additionally required to have a substantial transverse momentum of the muon jet $p_T^{\mu\mu} > 80$ GeV/c. This requirement dramatically improves the sensitivity of this topology for new physics signals that predict highly boosted muon jets. At the same time this requirement reduces acceptance for signal events containing only one dimuon per event, particularly for models with lower boosts of muon jets. For such models the sensitivity is driven by events in topologies with two or more dimuons per event, for which no high momentum requirement is imposed. Data events in topology R^1_2 with lower momentum dimuon candidates are used for background studies and validation of the background estimation techniques.

The only criteria used to identify and categorize signal topologies, other than the high-momentum

requirement applied to R_2^1, are the number of muon jets and the number and charge of muons within each muon jet. Muons that do not belong to any muon jet (which may arise from SUSY cascades, rather than dark photon decay) are neither used to identify nor to reject signal events. Other reconstructed objects, such as hadronic jets and missing energy, are neither selected nor rejected, even implicitly as an isolation cut. Of all possible combinations of N and n_i, only R_3^1, with low expected signal content, is not considered a signal. It is instead used as a control to test background parameterizations.

The background rates in the selected topologies are expected to be low with the exception of topology R_2^1, where backgrounds remain not negligible even after the $p_T^{\mu\mu} > 80$ GeV/c requirement. However, because the search for new resonances is performed in small windows in the invariant mass distribution of muon pairs, the rate of remaining background events in each window is at the level of a fraction of 1 pb, comparable to the rate of the signal if it is present in data. For topology R_2^1, the main SM background contributions are due to $b\bar{b}$ production with one of the b-quarks undergoing a double semi-leptonic decay, low-mass resonance production (prompt or from heavy flavor decays), low-mass Drell-Yan production, and occasional muon misidentifications due to decays-in-flight, either alone or in combination with a muon from the heavy flavor. For topology R_{22}^2, the SM backgrounds are dominated by the $b\bar{b}$ production with both b-jets undergoing double semileptonic decays or fragmenting into low-mass resonances decaying to pairs of muons. Background events with muon jets consisting of multiple muon candidates ("quadmuon" topology R_4^1 and the higher order topologies) typically originate from events with two muons from a b-jet and the other muons from either decays-in-flight, punch-through, or muon misidentifications where some of the segments from true muons are matched to the non-muon tracks. The SM content of the higher order regions is due to rare combinations of the causes discussed above and is extremely low.

To account for background contributions, we construct templates (one for each topology) modeling the distribution of reconstucted muon pair masses in background events. With the exception of the single dimuon topology R_2^1, the templates are multi-dimensional distributions in the $(m_1, ..., m_K)$ space of reconstructed muon pair masses, where K is the number of dimuons characteristic of a given topology. For each category, we define one or more background-enriched regions used to construct the template. In addition, we define a control region for validating the template using events with properties closely resembling those of the final events or using the off-diagonal side-band of the final $(m_1, ..., m_K)$ distribution.

While the templates were derived directly from data, we use simulation to determine the composition of the backgrounds as well as momentum evolution of certain parameters, e.g. the dimuon mass resolution and shape of the invariant mass distributions. To ensure that simulation is reliable in the phase space characteristic of this analysis, a series of detailed studies have been performed. First, the single-dimuon dataset with $p_T^{\mu\mu} < 80$ GeV/c (low momentum part of topology R_2^1) was divided in subsets dominated by one of the each contributing background prcocesses to measure rates, shapes, kinematic distributions, tracking related parameters and resolutions, mass resolutions of low-mass resonances as a function of boost, etc. These measurements were compared to simulation predictions showing very good agreement except a few known and well-understood shortcomings of the available simulated samples (lack of very low-mass Drell-Yan, missing production modes and/or dropped decay channels for some resonances).

To model the shape of the invariant mass distribution for the single dimuon region R_2^1, we define two sub-regions with $40 < p_T^{\mu\mu} < 60$ (background enriched region) and $60 < p_T^{\mu\mu} < 80$ GeV/c (control region). The first sub-region is used to obtain a parametrization of the shape

of the dimuon invariant mass distribution in background events shown in Fig. 1(a). To validate the template, we fit its shape (with the resolution of mass measurement evolved to higher $p_T^{\mu\mu}$) to the observed data in the sub-region $60 < p_T^{\mu\mu} < 80\,\mathrm{GeV}/c$, allowing only the overall normalization to float in the fit. The comparison shows good agreement as illustrated in Fig. 2(a). The same template (with mass resolution evolved to even higher $p_T^{\mu\mu}$) is used to predict the shape of background events of topology R_2^1 in the signal region $p_T^{\mu\mu} > 80\,\mathrm{GeV}/c$.

The SM backgrounds in the two-dimuon topology R_{22}^2 are dominated by $b\bar{b}$ events with each b-quark yielding a pair of muons. Because each b-jet fragments independently, the background distribution in the (m_1, m_2) space of the two dimuon masses is a Cartesian product of the 1D dimuon mass distribution with itself. However, because one of the dimuons contains the $p_T > 15\,\mathrm{GeV}/c$ muon that triggered the event, its dimuon mass spectrum is different from that of the other dimuon. To acount for this effect, we separately measure the shapes for the "trigger" and non-trigger dimuons. To model the "trigger dimuon" shape, we use single-dimuon events with further selections suppressing the non-$b\bar{b}$ backgrounds, fit to a parameterized functional form, subtracting residual contamination from Drell-Yan (both subtracted and non-subtracted curves are shown in Fig. 1(b)). To match the kinematics of the two-dimuon events being modeled, the "other dimuon" shape is obtained using three-muon events with a dimuon recoiling off a trigger-quality muon and is shown in Fig. 1(c). To properly account for a contribution with both dimuons containing a trigger-quality muon in the final 2D template, an additional re-weighing is applied in taking the Cartesian product of the two distributions. The template is validated using final two-dimuon events in the off-diagonal part of the (m_1, m_2) distribution. Figure 2(b) shows a comparison of the invariant mass distribution of the dimuons in these events (note that there are two histogram entries per event), compared to the prediction derived from the template and fit to the data for overall normalization only.

The quadmuon topology R_4^1 has a small background contamination in which a b-quark produces two real muons and an additional two muons are produced from from non-muon tracks incorrectly matched to some of the real muons' stubs. When identifying the two fundamental dimuons within the group of four muons, both $(\mu,\mu)+(trk,trk)$ and $(\mu,trk)+(\mu,trk)$ pairings can occur, each having its own distinct 2D shape in the (m_1, m_2) space. To model these events, we use single dimuon events and construct "pseudo mu-jets" using two reconstructed muons and two non-muon tracks playing the role of misidentified muons. Selected events are separated into two subsets according to the type of pairing, each producing a 2D distribution for the invariant masses of the two pairs in the event. Figures 1(d), (e) and (f) show 1D invariant mass distributions for (μ,μ), (trk,trk), and (μ,trk)-type dimuons obtained from projections of the 2D distributions for the two types of events. In the R_4^1 signal events, the identities of μ and trk are unknown, so the mass templates and the signal events are both symmetrized by randomly assigning dimuon masses to the horizontal and vertical axes of the plot. The template is validated using a control region with three nearby muon candidates (R_3^1), one of which is likely a misidentified hadron, and adding a non-muon track to play the role of a second misidentified muon. Figure 2(c) compares the distribution of all "dimuons" in the 3μ+track control sample (note two entries per event) compared to the prediction based on the full 2D template fitted to data for overall normalization only. Figure 2(d) makes a similar comparison but for the quadmuon invariant mass. Templates for higher order topologies are derived as combinations of the above methods. In all cases, the full posterior density functions for fit parameters including correlations were saved to be used in the final fit to account for the uncertainties in the background templates.

As mentioned above, the shapes of the invariant mass distribution for signal events was studied by comparing the properties of events with dimuons from ω, ϕ, J/ψ and ψ' resonances in

data with the simulation predictions and extrapolating between the resonance masses. Because of the excellent resolution of the CMS tracker, signal shapes have narrow width scaling with the mass of the resonances, with a slight dependence on the dimuon transverse momentum. For final fits, signal shape is parameterized using a Crystal Ball function with core resolution of $\sigma(m) = (0.026 + 0.0065\,m)$ GeV/c^2 (for barrel $|\eta^{\mu\mu}| < 0.9$) and $(0.026 + 0.013\,m)$ GeV/c^2 (for endcap $0.9 < |\eta^{\mu\mu}| < 2.4$). Multi-dimensional distributions were obtained by taking appropriate Cartesian products. The uncertainties on the parameters of the function are obtained by quantifying the level of agreement between data and simulation, which is dominated by the statistical uncertainties due to the size of samples reduced by the requirement of an appreciable boost. For dimuons with $p_T^{\mu\mu} < 150$ GeV/c, the reconstruction efficiency in the barrel region is nearly flat, is on average $95 \pm 1\%$, and is driven by the efficiency in the finding and matching stubs in the muon system. The efficiency decreases to about 92% for $m(\mu\mu)$ close to $2m_\mu$ due to muon trajectories becoming nearly collinear. In the endcap region, there is a slight lowering of efficiency towards high $|\eta|$ due to muon trajectories overlapping in the muon system. The systematic uncertainty on the efficiency in he endcap region is 3%. For higher-momentum dimuons, tracking effects become important as the overlaps of the trajectories leads to high sharing of hits and decreased efficiency. The effect is especially pronounced for $m(\mu\mu)$ of 0.4–0.6 GeV/c^2, where the efficiency decreases to $85 \pm 5\%$ at $p_T^{\mu\mu} \sim 250$ GeV/c and to $75 \pm 10\%$ at $p_T^{\mu\mu} \sim 350$ GeV/c due to "cowboy"-type events, in which muon trajectories bend towards each other in the magentic field and remain close to each other for a substantial part of their paths through the tracker. For muon pairs with $m(\mu\mu)$ outside of this range, the efficiency is nearly flat until 250 GeV/c^2, where it starts a slow descent towards higher momentum, being about 85 ± 5 at $p_T(\mu\mu) \sim 350$ GeV/c. The above-quoted uncertainties account for possible inaccuracies in modeling the size of the tracker hit clusters in the silicon tracker, which could affect the rate of merging hits from nearby tracks, driving the inefficiency of track reconstruction.

Reconstruction of quadmuons, e.g. produced via $h_d \to \gamma_d\gamma_d \to 4\mu$, suffers more significantly from reconstruction failures in the muon system. In addition to the 3% inefficiency per muon, quadmuon efficiency has a significant additional term related to small uninstrumented gaps beween the wheels of the muon system. With an inefficiency of 8–10% per muon crossing the gap region and a significant probability for one or more muons to cross it, the average reconstruction efficiency for a quadmuon is $83 \pm 3\%$. For high-momentum quadmuons, where tracking effects become more significant, the efficiency is determined by the probability to reconstruct each of the two low-mass dimuons comprising the quadmuon as the overlaps of muons from different dimuons are rare. Momentum dependence of the quadmuon efficiency closely follows the reconstruction efficiency of a dimuon with momentum equal to the higher-momentum dimuon within the quadmuon. It also has the same dependency on the invariant mass of the dimuons within the quadmuon. For a quadmuon with constituent dimuon mass of about 0.5 GeV/c^2 (the worst-case scenario), the average efficiency at $p_T^{\mu\mu\mu\mu} \sim 350$ GeV/c is about 76% and has a systematic uncertainty of 2–3% due to the tracking effect. Higher-multiplicity muon jets have larger inefficiencies due to muon system reconstruction failures, but would be reconstructed as lower-multiplicity jets. In the context of a specific model, the migration of events between the high-multiplicity topologies does not reduce the overall acceptance. Higher-multiplicity muon jet reconstruction is less affected by tracking inefficiencies as the average momentum of dimuons is moderate, even for very high momentum ($p_T^{\mu-jet} > 400\,\text{GeV}/c$) muon jets.

4 Results

The data in the regions used to search for signal (the "diagonal" regions of multi-dimensional distributions and the single-dimuon events with $p_T^{\mu\mu} > 80$ GeV/c) were hidden from the analyzers until all analysis selections and signal extraction techniques were finalized. When the signal regions were revealed, no evidence of new resonance production was found within the sensitivity of this analysis. Figure 3 shows the observed data for select topologies and the expted SM background contributions, which were obtained using the templates for each topology. The templates were normalized to the data in the off-diagonal regions in high-multiplicity topologies (all but R_2^1) and directly fitted in a combined signal-plus-background fit for the single-dimuon case (R_2^1). No events were found in any topologies with more than four muons.

To interpret the results in a model-independent fashion, we set the 95% C.L. upper limits on the alowed production rate of single-dimuon+X, quadmuon+X and two-dimuons+X topologies. The rate is defined as the cross-section times appropriate branching fractions to produce a particular signature times kinematical and geometrical acceptance (muon momentum thresholds and η ranges), assuming an ideal detector. Limits are set using Bayesian technique including integration over the systematic uncertainties in the signal and background shape parameterizations and the background normalization, which are treated as nuisance parameters. The limits shown in Fig. 4 account for instrumental inefficiencies as well as variations in reconstruction efficiencies for dimuon masses ranging from 0.25 to 5 GeV/c^2 and the mean of the muon jet (dimuon or quadmuon) momentum distributions up to 250 GeV/c. These variations were treated as an additional systematic uncertainty and were 7% for the quadmuon topology, 20% for dimuon, and 35% for two dimuon topology. For higher momentum muon jets, the limits would become weaker due to diminishing reconstruction efficiency. Other systematic uncertainties account for the accuracy in the luminosity measurement (4%), uncertainties in the efficiency of reconstructing and matching muon stubs to the tracks and triggering (1-4% depending on the topology), and track reconstruction efficiency (5-10%). The presented quadmuon+X limit can be used as a lower bound on signals with muon jets containing four or more muons in it. Note that these limits are conservative in the sense that they assume that reconstruction failures always exclude events from consideration while in realistic models reconstruction failures cause events to be reconstructed in one of the lower multiplicity topologies.

To set limits for representative benchmark scenarios, we use two models for SUSY with the dark sector. The first SUSY model [5] assumes standard MSSM squark/gluino production and cascades followed by the decay of the MSSM LSP into the dark sector $\chi_1^0 \to h_{\rm dark}\chi_{\rm dark}$ or $\chi_1^0 \to \gamma_{\rm dark}\chi_{\rm dark}$, where $\chi_{\rm dark}$ is the new cold dark matter candidate. The dark sector masses used are $m(h_{\rm dark}) = 3$, $m(\gamma_{\rm dark}) = 0.5$, and $m(\chi_{\rm dark} = 300$ GeV/c^2. The resulting limits are shown as a function of gluino mass $m(\tilde{g})$ ($m(\tilde{q}) = m(\tilde{g})/1.2$ for first two generations) in Fig. 4(b) for three different choices of branching fractions $B(\gamma_{\rm dark} \to \mu\mu)$. In addition to the systematic uncertainties used for model-independent limits, we include the uncertainty of 3% in the acceptance to account for uncertainties in PDFs by varying parameterizations within the CTEQ6.6 [21] family, and comparing central values of CTEQ6.6L with NNPDF2.0 [22], and MSTW2008 [23] sets). The second model [6] assumes squarks to be the standard MSSM LSP ($m(\tilde{q}) = m(\tilde{g})/1.2$). Following production, squarks decay via $\tilde{q} \to qn_2$, where n_2 is a heavier dark sector fermion with the decay modes dominated by either $n_2 \to n_1\gamma_{\rm dark}$ or $n_2 \to n_1 h_{\rm dark}(\to \gamma_{\rm dark}\gamma_{\rm dark})$. For each of the two sub-models the limits on the production cross-section are shown in Fig. 4 (c) and (d) for three different choices of branching fractions $B(\gamma_{\rm dark} \to \mu\mu)$. The dark sector masses are set to $m(h_{\rm dark}) = 1.2$, $m(h_{\rm dark}) = 0.5$, $m(n_2) = 2$, $m(n_1) = 0.5$ GeV/c^2. The cross section curves shown in Figs. 4(b-d) assume universality of

squark masses across all three generations and therefore can be substantially lower if those are not universal. These limits are the most stringent limits for models with dark SUSY sector from collider experiments.

Finally, we consider a model with the NMSSM higgs production decaying via $h_1 \to a_1 a_1$. If $m(a_1) < 2m_\tau$, a_1 has a significant branching fraction for decays into a pair of muons. The sensitivity of this analysis to $\sigma(pp) \to h_1 \to a_1 a_1 \to (\mu\mu)(\mu\mu)$ is dominated by the two-dimuon region R^2_{22} leading to a 95% C.L. limit on the production rate of about 0.2 pb. To interpet the limit in the context of the allowed NMSSM models, we follow [19] to generate a series of the NMSSM model points with $m(a_1) < 2m_\tau$ and consistent with the WMAP and LEP data. For each point we calculate the LHC production cross-section for h_1 and the branching fraction $B(h_1 \to a_1 a - 1 \to 4\mu)$, see Fig. 4(e). The bands shows the range of excluded model points (the limits are not strict curves in this plot because different model points have different acceptance depending on the masses of $m(h_1)$ and $m(a_1)$). On the same plot we show an exclusion band for a similar Tevatron analysis [18].

5 Conclusions

A signature-based search for groups of collimated muons (muon jets) in the first 35 pb^{-1} of the LHC data collected by the CMS experiment has revealed no signals of new physics within the sensitivity of the measurement. We found zero events consistent with two or more decays of the predicted new light boson species to a pair of muons in the same event, and no excess over the SM backgrounds for production of single high-p_T bosons decaying to pair of muons. Relaxing the assumption that the light bosons are on-shell and searching for possible $a_2 \to a_1 a_1 \to 4\mu$ cascades revealed one event, consistent with the background expectation.

With these observations, we set limits on the production of new low-mass states decaying to pairs of muons that can be applied to a broad class of models predicting the lepton jet signatures. These limits exclude production of new physics in several event topologies with 95% C.L. limits on $\sigma \times \mathcal{B} \times \alpha_{\text{gen}}$ in the range of 0.1–0.5 pb.

We also set model-dependent limits on several benchmark models predicting production of the new light states in the context of Dark SUSY, which significantly extend the reach of the Tevatron analyses to these kind of signatures. In the context of the NMSSM Higgs search in the channel $h \to a_1 a_1 \to 4\mu$ with $m(a_1) < 2m_\tau$, the LHC senstivitity will surpass that of the Tevatron experiments with 100 pb^{-1} of data and will significantly constrain the allowed NMSSM parameter space with 1 fb^{-1} of data.

References

[1] O. Adriani et al., "Observation of an anomalous positron abundance in the cosmic radiation", *Nature* **458** (2009) 607–609.

[2] O. Arkani-Hamed et al., "A Theory of Dark Matter", *Phys. Rev.* **D 79** (2009) 015014.

[3] R. Bernabei et al., "New results from DAMA/LIBRA", *Eur. Phys. J.* **C 67** (2010) 39–49.

[4] P. J. Fox and E. Poppitz, "Leptophilic Dark Matter", *Phys. Rev.* **D 79** (2009) 095023.

[5] Y. Bai and Z. Han, "Measuring the Dark Force at the LHC", *Phys. Rev. Lett.* **103** (2009) 051801.

[6] J. T. Ruderman, W. M. Maumgart, C. Cheung et al., "Non-abelian dark sectors and their collider signatures", *JHEP* **04** (2009) 014.

[7] H. P. Nilles, M. Srednicki, and D. Wyler, "Weak Interaction Breakdown Induced By Supergravity", *Phys. Lett.* **B 120** (1983) 346.

[8] J. M. Frere, D. R. T. Jones, and S. Raby, "Fermion Masses And Induction Of The Weak Scale By Supergravity", *Nucl. Phys.* **B 222** (1983) 11.

[9] J. R. Ellis, J. F. Gunion, H. E. Haber et al., "Higgs Bosons in a Nonminimal Supersymmetric Model", *Phys. Rev.* **D 39** (1989) 844.

[10] M. Drees, "Supersymmetric Models with Extended Higgs Sector", *Int. J. Mod. Phys.* **4** (1989) 3635.

[11] U. Ellwanger, M. Rausch de Traubenberg, and C. A. Savoy, "Particle spectrum in supersymmetric models with a gauge singlet", *Phys. Lett.* **B 315** (1993) 331.

[12] U. Ellwanger, M. Rausch de Traubenberg, and C. A. Savoy, "Higgs phenomenology of the supersymmetric model with a gauge singlet", *Z. Phys.* **C 67** (1995) 665.

[13] D. J. Miller, R. Nevzorov, and P. M. Zerwas, "The Higgs sector of the next-to-minimal supersymmetric standard model", *Nucl. Phys.* **B 681** (2004) 3.

[14] J. E. Kim and H. P. Nilles, "The Mu Problem And The Strong CP Problem", *Phys. Lett.* **B 138** (1984) 150.

[15] G. o. O. C. Abiendi *EPJC* **27** (2003) 483–495.

[16] V. Abazov and others (DØ Collaboration), "Search for Dark Photons from Superseymmtric Hidden Valleys", *Phys. Rev. Lett.* **103** (2009) 081802.

[17] V. Abazov and others (DØ Collaboration), "Search for Events with Leptonic Jets and Missing Transverse Energy in $p\bar{p}$ collisions at $\sqrt{=}$1.96 TeV", *Phys. Rev. Lett.* **105** (2010) 211802.

[18] V. Abazov and others (DØ Collaboration), "Search for NMSSM Higgs bosons in the h-¿aa-¿mumu mumu, mumu tautau channels using ppbar collisions at $\sqrt{s} = 1.96$ TeV", *Phys. Rev. Lett.* **103** (2009) 061801.

[19] A. Belyaev, J. Pivarski, A. Safonov et al., "LHC discovery potential of the lightest NMSSM Higgs in the $h_1 \to a_1 a_1 \to 4\mu$ channel", *Phys. Rev.* **D 81** (2010) 075021.

[20] CMS Collaboration, "The CMS experiment at the CERN LHC", *JINST* **0803:S08004** (2008).

[21] P. Nadolsky et al., "Implications of CTEQ global analysis for collider observables", *arxiv:0802.0007* (2008).

[22] R. Ball et al., "A first unbiased global NLO determination of parton distributions and their uncertainties", *arXiv:1002.4407* (2010).

[23] A. Martin, W. Stirling, R. Thorne et al., "Parton distributions for the LHC", *Eur. Phys. J* **C 63** (2009) 189–285.

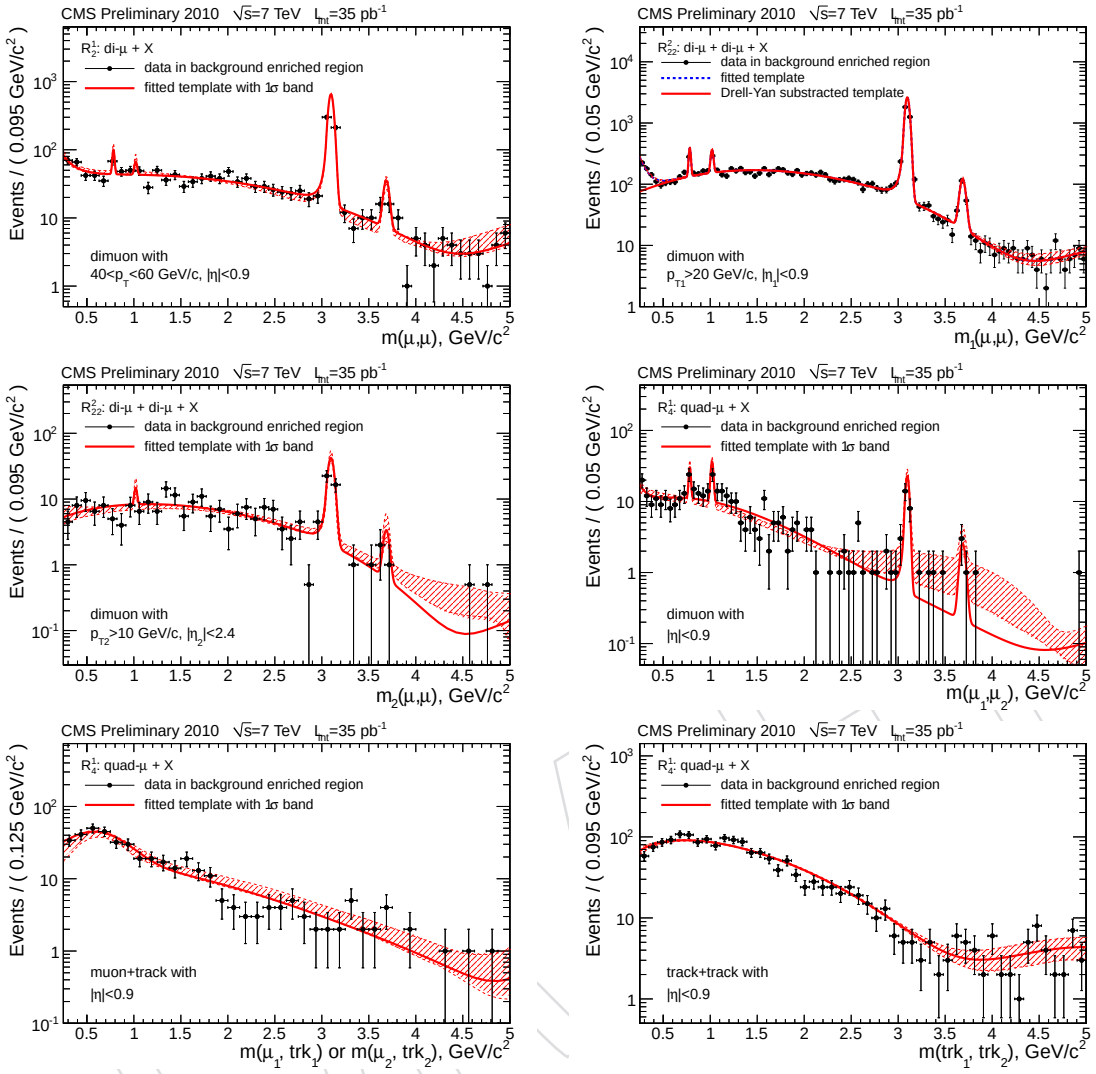

Figure 1: Dimuon invariant mass distributions in the background-enriched samples for different topologies. The data are overlaid with parameterized functions, fitted to the data. These are used to construct mass-shape templates for the distributions of background events in signal regions. Background templates for topologies with high muon multiplicity are modeled as Cartesian products of these distributions. (a): Distribution of the single-dimuon events (topology R_2^1) with $40 < p_T^{\mu\mu} < 60$ GeV/c. (b): Distribution of dimuon events containing a trigger-quality muon ($p_T > 15$ GeV/c and $|\eta| < 0.9$) used to model the invariant mass shape of the "first" dimuon candidate in the two-dimuon topology R_{22}^2. (c): Dimuon invariant mass distribution for events with a dimuon candidate and an additional, unclustered, trigger-quality muon, used to model the distribution of the "second" dimuon in background events in topology R_{22}^2. (d), (e) and (f): Distributions of the "dimuon" invariant mass in events with two muons and two tracks playing the role of misidentified muons in quadmuon topology R_4^1, for the cases when the dimuon is reconstructed from two true muons, one true muon and a track, and two tracks emulating misidentified muons, respectively.

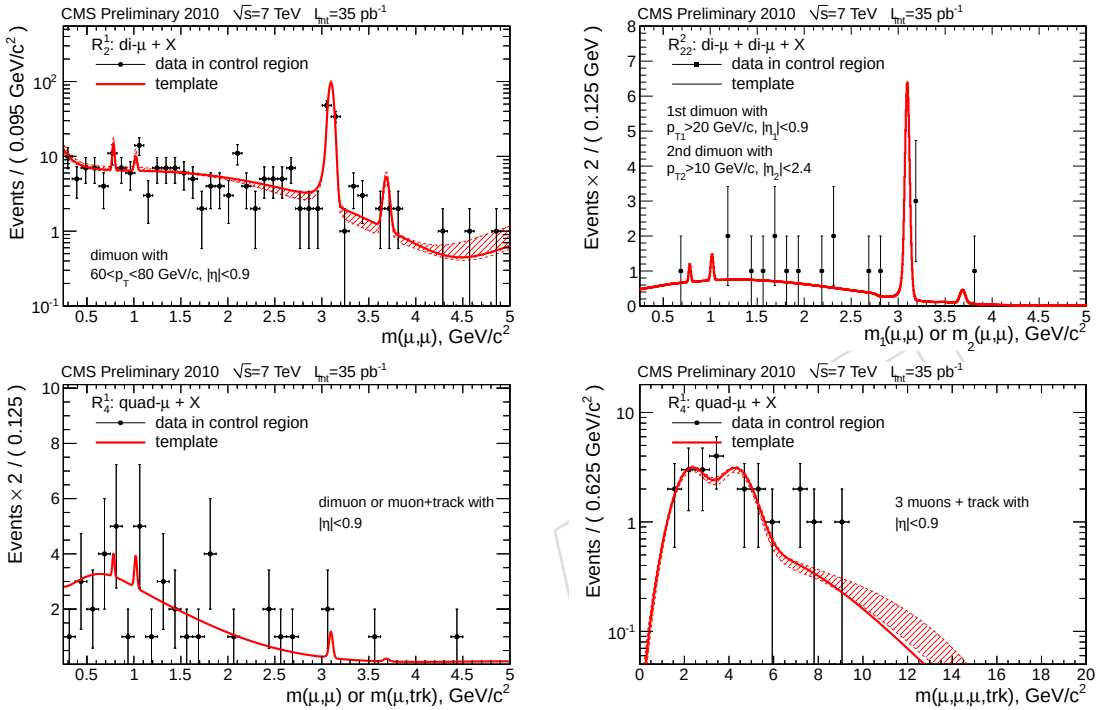

Figure 2: (a): Data in the single-dimuon category (R_2^1) control region $60 < p_T^{\mu\mu} < 80$ GeV/c overlaid with the background prediction obtained from the background-enriched region $40 < p_T^{\mu\mu} < 60$ GeV/c, fitted for overall normalization only. (b): The invariant mass of all dimuons in the off-diagonal region for events in the two-dimuon category (R_{22}^2, note that there are two entries per event), compared with the prediction obtained from the full 2D background template, fitted for overall normalization only. (c): The invariant mass distribution of all "dimuons" in the 3μ+track events (two entries per event) used as a control region for the analysis of events in the quadmuon category (R_4^1). The distribution is compared with the prediction obtained from the full 2D background template, fitted for overall normalization only. (d): The invariant mass of of the four "muons" in the 3μ+track control region for the quadmuon topology R_4^1 compared with the prediction obtained from the data in the background-enriched region ($2\mu + 2$tracks).

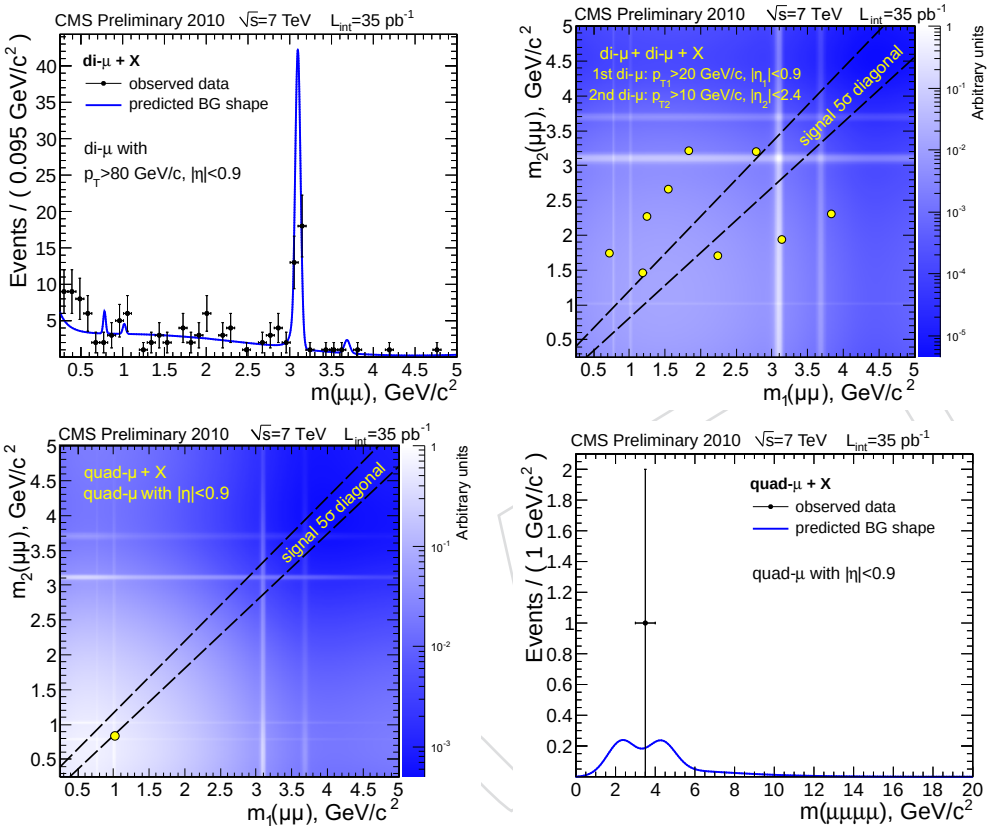

Figure 3: 2D and 1D invariant mass distributions of muon pairs for events in each signal region, compared with the expected background: "single dimuon" events in topology R_2^1 (a), 10 events in the "two-dimuon" topology R_{22}^2 (b), the single "quadmuon" event in topology R_4^1, (c) and the invariant mass of all four muons for the same event (d). None of the events in the the multi-dimensional topologies fall into the corridor along the diagonal (shown as dashed lines), which would indicate the presence of signal. The last plot is relevant for the special scenario with a cascade decay $a_2 \to a_1 a_1$ with $m(a_2) < 2m(a_1)$, leading to the off-shell production of a_1.

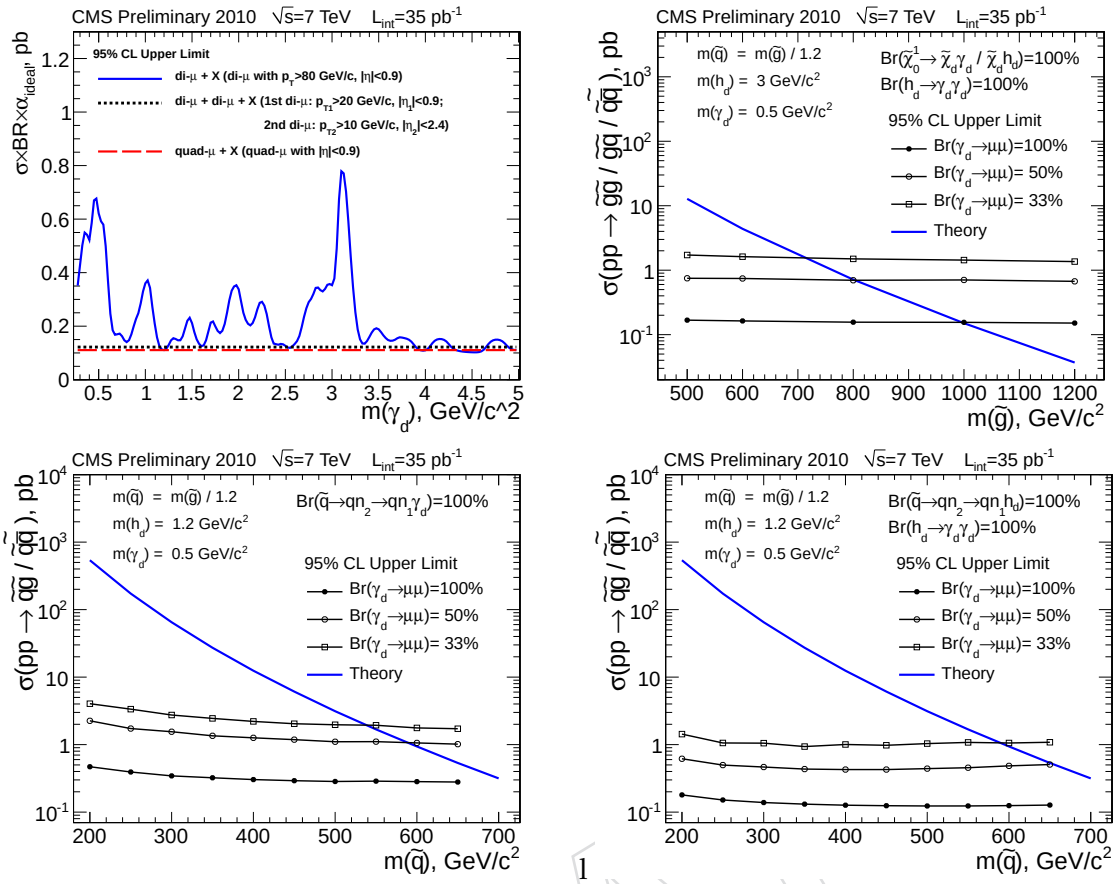

Figure 4: (a) 95% C.L. upper limits on the rate of the signals of new physics with lepton jets for three topologies. (b) Limits for the Dark SUSY model with the MSSM LSP decaying via $\tilde{\chi}_1^0 \to \tilde{\chi}_d\gamma_d + \tilde{\chi}_d h_d(\to \gamma_d\gamma_d)$, with the $\tilde{\chi}_d$ being the cold dark matter candidate (c) and (d): limits on the model where squark is the MSSM LSP decaying into a quark and a light hidden sector fermion decaying to a lighter hidden sector fermion with emission of either a dark photon or a light dark higgs decaying to two dark photons.

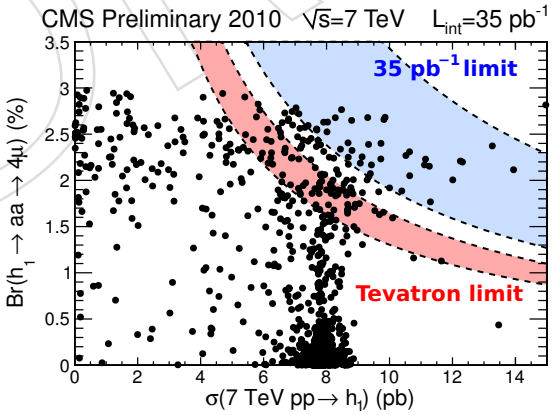

Figure 5: The NMSSM models consistent with WMAP and LEP higgs constraints (shown as points) compared to the exclusions obtained by setting a 95% C.L. upper limits on the higgs production via the $h_1 \to a_1 a_1 \to 4\mu$ channel in this analysis and in the Tevatron searches. Both searches exclude the upper right corner of the parameter space, exclusion limits depend on the exact masses of h_1 and a_1 and therefore are shown as bands corresponding to mh_1 varied from 89 to 120 GeV/c^2 and $m(a_1)$ varied from $2m(\mu)$ to $2m(\tau)$.